Ceramics International xxx (xxxx) xxx–xxx

Contents lists available at ScienceDirect

Ceramics International

journal homepage: www.elsevier.com/locate/ceramint

Evolution of microstructure and nanohardness of SiC fiber-reinforced SiC matrix composites under Au ion irradiation

Chao Ye[a,b,c], Jiaxiang Xue[d], Tong Liu[d,**], Rui Shu[d], Yan Yan[d], Yehong Liao[d], Qisen Ren[d], Guang Ran[a,b,***], Kai Sun[e], Li Jiang[c], Pengyuan Xiu[c], Lumin Wang[c,e,*]

[a] College of Energy, Xiamen University, Xiamen, Fujian, 361102, China
[b] Fujian Research Center for Nuclear Engineering, Xiamen City, Fujian Province, 361102, China
[c] Department of Nuclear Engineering and Radiological Sciences, University of Michigan, Ann Arbor, MI, 48109, United States
[d] China Nuclear Power Technology Research Institute Co., Ltd, Shenzhen, 518000, China
[e] Department of Materials Science and Engineering, University of Michigan, Ann Arbor, MI, 48109, United States

ARTICLE INFO

Keywords:
SiC_f/SiC composites
Microstructure
Ion irradiation
Nanohardness

ABSTRACT

Evolution of microstructure and nanohardness of a new type of SiC_f/SiC composite under a 6 MeV Au ion irradiation up to 90 displacements per atom at 400 °C was studied. Scanning transmission electron microscopy reveals that the irradiation has induced enrichment of carbon at the grain boundaries in the fibers. This is attributed to the accumulation of C interstitials generated by the irradiation. The disappearance of {200} diffraction ring of 3C–SiC indicates that a phase transition from 3C–SiC to Si has occurred during irradiation. In addition, the hardness of SiC fiber increased after irradiation, which is due to the pinning effect caused by irradiation-induced defects. The pyrolytic-carbon interphase that contains Si-rich nano-grains in the composite has the highest irradiation tolerance as it maintained its basic morphology and graphitic nature after a radiation damage dose up to 90 dpa. Twins are the main internal defects in the SiC matrix of the SiC_f/SiC composite, which grew up and resulted in the decrease of the number of twinning boundaries under irradiation. No significant microstructure change has been observed in the SiC matrix except a limited number of dislocation loops at the peak irradiation damage region. The entire matrix still maintained its hardness after irradiation.

1. Introduction

Due to its perfect high-temperature stability [1], creep resistance [2], excellent irradiation resistance and low neutron capture cross-section [3], silicon carbide (SiC) is known to be a promising material used as the structural support components in TRISO nuclear fuel and the next generation fuel cladding in advanced tolerant fuel [4,5]. As the inherent low toughness problem of SiC, the SiC fiber-reinforced SiC matrix (SiC_f/SiC) composite was developed as a fuel cladding material [6–8].

A SiC_f/SiC composite usually consists of SiC fibers, pyrolytic carbon (PyC) interlayer and SiC matrix. The SiC matrix is usually deposited on the SiC fiber surface by several methods, including chemical vapour infiltration (CVI) [9,10], transient eutectic phase [11], melt infiltration [12,13] and precursor infiltration and pyrolysis [14]. Among these methods, CVI is considered as the best choice to produce very high purity β-phase SiC, which has better radiation resistance than other phases of SiC [15]. The commercially available Tyranno SA3 (TSA) and Hi-Nicalon Type S (HNS) fibers both contain equiaxed grains with the carbon precipitates at the grain boundaries and the size of the fiber grains is more than 50 nm [1,16]. Weber [16] and Kondo [17] et al. revealed that ion irradiation could induce the loss or annihilation of the pre-existing carbon packets in the fibers resulting in the fiber shrinkage. They proposed that the disappearing carbon entered the interior of the SiC grains. The PyC interlayer that deposited outside the fibers are used to enhance the dimensional stability of fibers [18] that remained stable after 10 MeV Au ion irradiation [16]. Snead et al. found that the loss of PyC interphase due to the neutron irradiation could lead to the degradation of the mechanical properties of the fiber/matrix interface [19]. In addition, the inter-diffusion enhanced by irradiation of silicon atoms between the PyC and SiC was reported [17]. For unirradiated SiC_f/SiC composite materials, previous studies have shown that the

* Corresponding author. Department of Nuclear Engineering and Radiological Sciences, University of Michigan, Ann Arbor, MI, 48109, United States.
** Corresponding author. China Nuclear Power Technology Research Institute Co., Ltd, Shenzhen, 518000, China.
*** Corresponding author. College of Energy, Xiamen University, Xiamen, Fujian, 361102, China.
E-mail addresses: liutong@cgnpc.com.cn (T. Liu), gran@xmu.edu.cn (G. Ran), lmwang@umich.edu (L. Wang).

https://doi.org/10.1016/j.ceramint.2019.12.044
Received 4 October 2019; Received in revised form 20 November 2019; Accepted 3 December 2019

hardness of the SiC matrix is higher than that of the SiC fiber, which is due to the existence of carbon packets [1,20]. In addition, previous studies indicated that different SiC fiber types would have different hardness changes after irradiation. For example, the hardness of 601–4 SiC fiber gradually decreased with increasing ion fluence, while the hardness of Tyranno SA SiC fiber firstly increased and then decreased with the increase of ion fluence [21].

As the overall properties of a composite are determined by the properties of the constituents and interaction between them, it is necessary to evaluate the performances of the SiC_f/SiC composite before and after irradiation. It has been one of the most interesting topics nowadays to study irradiation effect on the performance of the SiC_f/SiC composites. Compared with the previous studied SiC_f/SiC composites, we studied a new type of SiC_f/SiC composite with different internal microstructures. In this study, high-resolution scanning transmission electron microscopy (STEM) observation and nanohardness tests were made for the SiC_f/SiC composite before and after irradiation to correlate the relationship between hardness and microstructure.

2. Experimental

The SiC_f/SiC composite materials used in this study were prepared by CVI process. Two-dimensional woven SiC fabrics were used for the preparation of this material. The PyC, selected as fiber/matrix interface, was deposited on the SiC fabric with a thickness about 150 nm. The SiC matrix was deposited by CVI process using methyltrichlorosilane (MTS, CH_3SiCl_3) and hydrogen as the precursors at a temperature of 1000 °C with a pressure of 5 kPa. The molar ratio of MTS/H_2 was 10, and the deposition time was 72 h for each CVI cycle.

For irradiation experiment, the composites were sliced into 1.5 mm thick pieces perpendicular to the fiber axis using a diamond cutting saw, followed by mechanical polishing with a 0.5 μm diamond sandpaper. The sample dimensions for irradiations were 3 mm × 10 mm x 1 mm. The irradiation experiment was performed in a multi-purpose target chamber using a 3.0 MV tandem accelerator at the Ion Beam Radiation Laboratory at the University of Michigan. The ion irradiations were conducted using 6 MeV Au ions at 400 °C with the ion fluences up to 2.5×10^{16} ions. cm^{-2}. As it is known that about 90% of the initially formed vacancies and interstitials recombine during implantation as a consequence of the elevated implantation temperature [22], the elevated implantation temperature is in order to minimize the implantation damage and no amorphization is expected. The displacement threshold energies of 35 eV and 20 eV for Si and C [23], respectively, were set in the Stopping and Range of Ions in Matter (SRIM) simulation software based on Full Damage Cascades mode. The material density used in the SRIM calculations was 3.21 g/cm^3. The results of the depth variation of damage and Au concentration are shown in Fig. 1. Instead of using self-ions (Si^+ or C^+), the irradiations were performed with Au ions in this work. Apart from the relatively inert nature, Au ions also produce substantially more damage per incident ion. It is necessary to avoid implanting significant quantities of Si or C ions into the sample, which would induce injected interstitial artifacts [24] and affect the local elemental composition ratio and interfere with the determination of any chemical intermixing or segregation under the irradiation conditions. During the ion irradiation process, some parts of the samples were sheltered by masks to leave the areas underneath unirradiated for comparing to the irradiated ones.

The microstructure and composition were characterized by scanning electron microscopy (SEM), and STEM with energy-dispersive X-ray spectroscopy (EDS) and electron energy loss spectroscopy capabilities. STEM specimens of less than 100 nm thick were prepared using a focused ion beam (FIB) lift-out technique with a FEI Helios 650 Nanolab FIB/SEM instrument at Michigan Center for Materials Characterization (MC^2). The initial lift-outs were performed using 30 kV Ga ions with the current of 9.3 nA. During thinning, the energy and current of Ga beam were progressively decreased to minimize

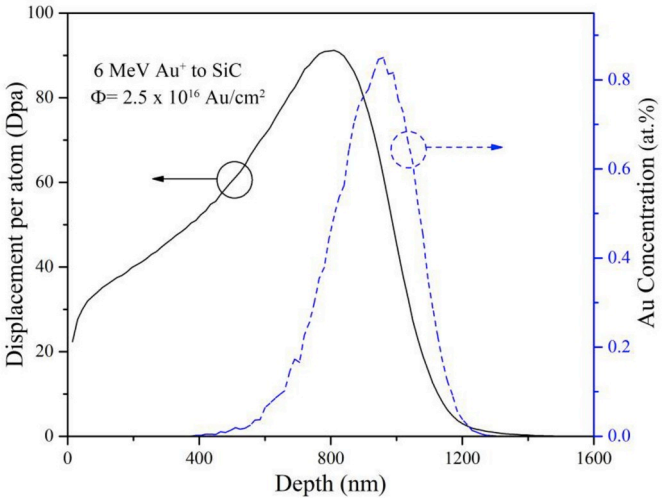

Fig. 1. Depth variation of displacements per atom (dpa) and Au concentration (at. %) in SiC after 2.5×10^{16} Au ions/cm^2 calculated by SRIM with Full Damage Cascades mode.

milling induced damage. Final thinning was performed using 2 kV Ga ions. Aberration corrected JEOL2100F TEM/STEM was utilized at 200 keV to characterize the FIB foils using conventional bright field (BF), dark field (DF) and EELS techniques.

Hardness measurements were performed at room temperature using a Hysitron TI950 Triboindenter. A standard transducer (maximum load is 10 mN, maximum displacement is 5 μm) with a Berkovich probe was used for the tests. All the samples were tested with a load control mode at the maximum load of 10 mN. Continuous hardness measurement was set for the samples with a constant loading rate $\dot{P}/P = 0.05/s$. For good statistical analysis, each sample was indented with at least 15 indents and the average data of the results were adopted.

3. Results and discussions

The general view of the polished surface of the SiC_f/SiC composite sample is presented in Fig. 2(a), a SEM secondary electron image (SEI). Many pores with different size are evident on the sample surface and some fibers marked with red arrows are parallel to surface. Fig. 2(b) presents a magnified SEI image giving a more detailed view of the fibers, which are perpendicular to the surface with the average diameter about 15 μm. At such a magnification, individual fibers can be easily resolved, which enables the precise aiming at the regions of interest (individual SiC fibers, SiC matrix or fiber coating regions) for micromechanical testing and lifting out the TEM specimens by FIB. The dark thin “halos” surrounding each fiber are pyrolytic carbon (PyC) interlayers. Outside the PyC interlayers, there are still multilayer SiC coatings. SiC fibers are uniformly embedded in the SiC matrix.

Cross-section STEM images of the sample are shown in Fig. 3, which present the microstructure inside the SiC_f/SiC composite clearly. In Fig. 3(a), the leftmost side is the SiC fiber with the white contrast PyC layer on its right side and the rightmost side is the SiC matrix. The SiC coating area between them consists of multiple layers with different contrast. Each area marked in Fig. 3(a) is consistent with the result of EDS line scan analysis in Fig. 3(b). In Fig. 3(b), the widest black contrast area is the PyC layer, whose EDS data shows that this region is mainly composed of carbon. Apart from the PyC layer, the EDS line profile image shows that there are two interface locations showing a significant reduction of the silicon composition, but the carbon content does not change significantly. As the multiple layers in SiC coating area were deposited in batches by CVI process, which resulted in that the content of silicon in the interface junction is relatively lower than the inside area of the coating. The relatively lower silicon content in the

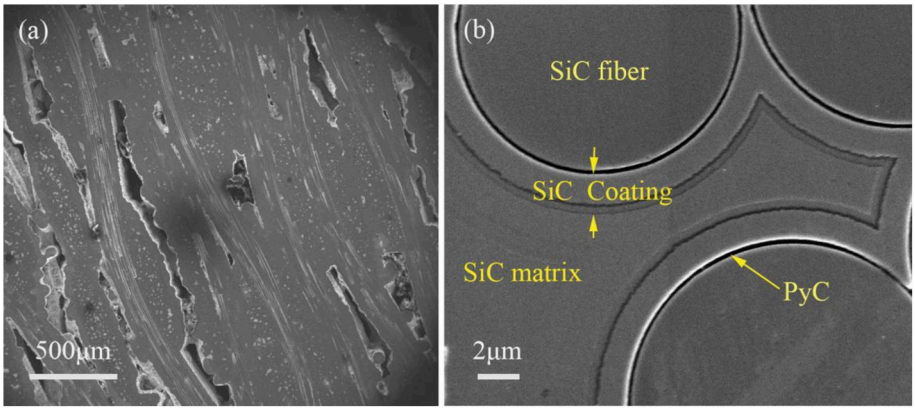

Fig. 2. SEM SEI images of the polished surface of SiC_f/SiC composite: (a) overview image; (b) enlarged image.

interface junction is due to the interruption between batches of the CVI process. It can be seen from Fig. 3(b) that the compositions of SiC coating and SiC matrix are very similar, but the content of silicon in SiC fiber is relatively lower than SiC coating and SiC matrix. The SiC fiber consists of nanocrystals; the SiC matrix consists of columnar crystals parallelling to the surface; and the SiC coating consists of both nanocrystals and columnar crystals.

3.1. The behavior of SiC fiber under irradiation

As shown in Fig. 4(a), the original SiC fiber has a nano-polycrystalline structure with the grain size ranging from 5 nm to 20 nm. From the enlarged image of Fig. 4(b), the lattice structure is clearly visible with some defects inside the grain, such as twins. The SiC fibers were seen to still maintain its polycrystalline structure after irradiation to 90 dpa with little change in grain size, as shown in Fig. 4(c). However, from the enlarged image Fig. 4(d) of the marked area in Fig. 4(c), it can be seen that this black contrast area contains small grains. As black contrast generally indicates that the grain orientation is just in the direction of the crystal zone under bright-field condition [25], this black contrast area might be originally a relatively larger grain and grain refinement occurred during the ion irradiation process [26]. In addition, we did not observe similar phenomenons in the non-irradiated SiC fiber area. Meanwhile, the average size of the grains in the irradiated area and the unirradiated area were calculated about to be 12.1 ± 1.6 nm and 14.6 ± 2.5 nm, respectively. More than 50 nanograins were analyzed, and all the grains were calculated and counted in high-resolution images.

Fig. 5(a) is a BF images of the unirradiated area in SiC fiber and Fig. 5(b) is the corresponding high angle annular dark-field (HAADF) image of the same area in Fig. 5(a), which shows the Z-contrast of materials [27]. In the SiC fiber-reinforced SiC matrix composite studied, the white contrast represents a higher content of heavier element Si and the black contrast represents a higher content of the lighter element C. The grain boundaries are often associated with inclusions, one of which is shown in Fig. 5(a) and (b) (HADDF mode, indicated by the red arrow). These inclusions show black contrast in the HADDF images implying enrichment of carbon [16]. However, different from the observations of previous reported SiC_f/SiC composites [28], the distribution of such inclusions in the current studied SiC_f/SiC composite is more uniform due to the different preparation processes and conditions. Fig. 5(c) and (d) are HADDF images from the unirradiated and irradiated fiber areas, respectively. Although there are also a large amount of black contrast areas in the unirradiated fibers (Fig. 5(c)), the contrast of the black areas in the irradiated fibers is significantly darker and the average size of these spots is also larger (Fig. 5(d)). This indicates that more C atoms have migrated to the nano-grain boundaries during the irradiation. The selected area electron diffraction (SAED) pattern shown in Fig. 5(d) as an inset taken from the irradiated SiC fiber does not show the 200 diffraction ring compared with that from the unirradiated SiC fiber area shown in Fig. 5(c) as an inset. This indicates that atomic rearrangement has occurred during the ion irradiation process, i.e., the zinc blende SiC structure has been transformed into a diamond structure resulting in the disappearance of the 200 diffraction ring, which is due to the loss of carbon atoms (Detail analysis can be seen in the supplemental file). The highlighted white spots that can be observed in Fig. 5(d) are the implanted Au atom clusters. As the content of implanted Au ions was extremely low, they uniformly dispersed in the SiC

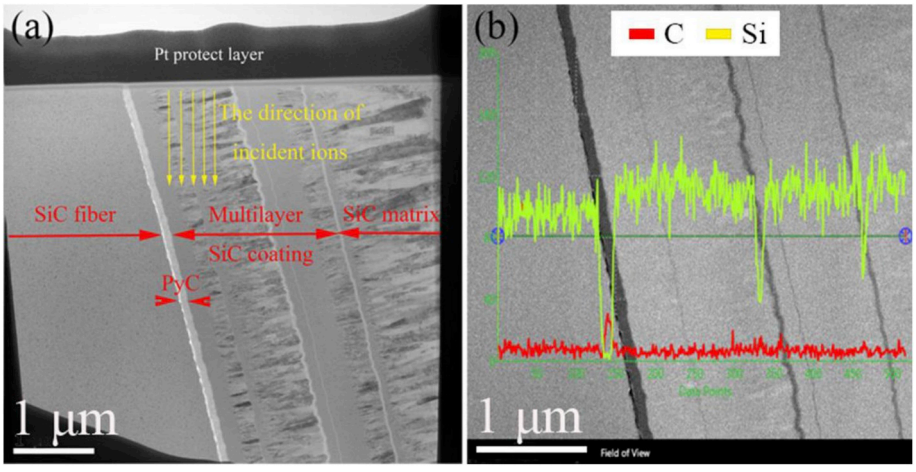

Fig. 3. STEM images of SiC_f/SiC composite: (a) Bright field; (b) ADF image with EDS line profiles overlapped.

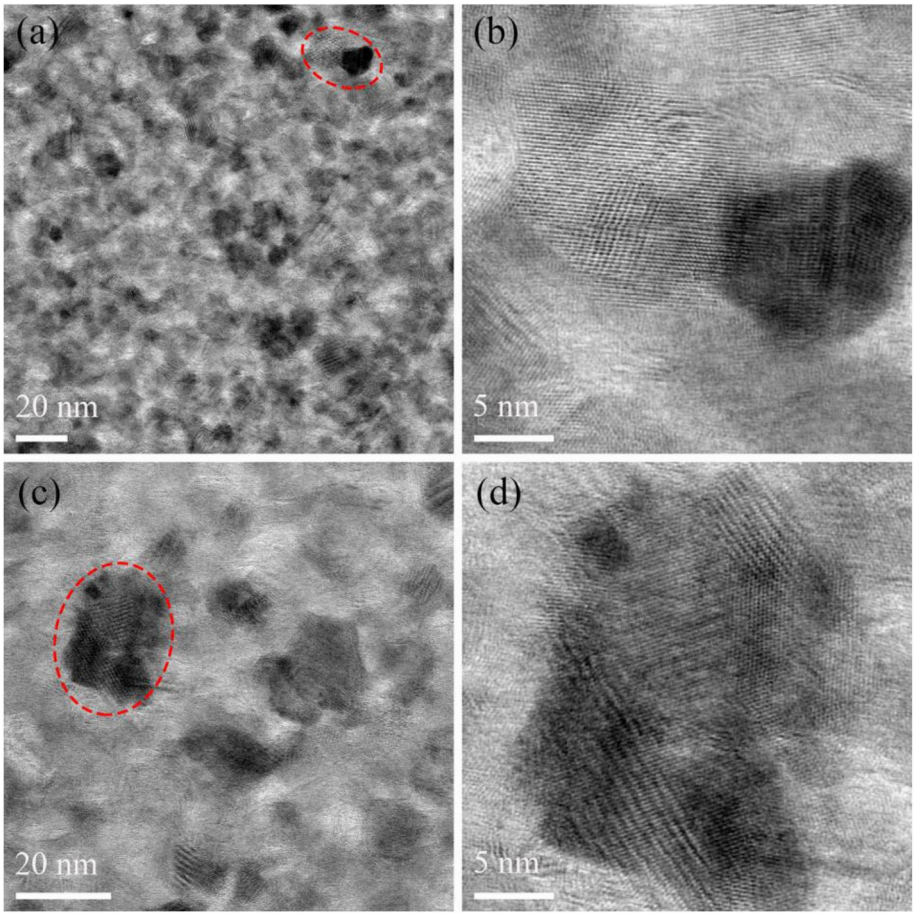

Fig. 4. STEM BF images of SiC fiber area: (a) unirradiated SiC fiber area; (b) an enlarged image of the marked area in (a); (c) irradiated SiC fiber area; (d) an enlarged image of the marked area in (c).

matrix without aggregating to form large precipitates. Element mapping by EELS was performed from both the irradiated and unirradiated samples, as shown in Fig. 6. It indicates the enrichment of C around the nanocrystals increased significantly, while the content of C inside the SiC nanocrystals seemed to decrease after irradiation in the fiber area. As the displacement threshold energies of C is less than Si, so a large number C interstitials were produced during the irradiation process. The formation energy for the C vacancy-interstitial pair was established to be 5.1 eV [29], while the migration energy for C interstitials has been found to be about 1 eV (at least for positive and neutral charge states) [30], which enables the C interstitials to migrate over large distances before being trapped during the irradiation process. This might be the reason why the C enriched at the boundaries of the nanocrystals after irradiation. The evolution phenomenon of carbon packets in the studied SiC_f/SiC composite after irradiation is different from the SiC_f/SiC composites with TSA and HNS fibers [1,16,18]. However, neutron irradiations experiments for SiC_f/SiC composites made by Perez-Bergquist et al. showed the similar results that a size increase of intergranular carbon packets in SiC_f/SiC composite made with HNS fibers [31]. The grain size of SiC fibers in the current SiC_f/SiC composite is about 10 nm, while the grain sizes of TSA and HNS fibers are more than 50 nm. It can be speculated that the grain size, the distribution and density of carbon packets in the fiber might affect the migration and aggregation of carbon during the ion irradiation in the SiC fibers.

3.2. The behavior of pyrolytic carbon under irradiation

PyC layer is about 150 nm thick, as shown in Fig. 3. Pyrolytic carbon normally exists in the form of amorphous status [32] that should show a homogenous contrast in STEM images. However, the STEM BF image in Fig. 7(a) shows the formation of small crystal grains with few nanometers in the PyC layer with some marked by red arrows. Fig. 7(b) is a HAADF image from the same area in Fig. 7(a) showing bright contrast areas, which are consistent with the small crystal particles in Fig. 7(a). EDS element profiles across these areas show that such particles contain silicon element, which suggests that some small crystal grains of SiC or Si are dispersed in the PyC layer. Some research results indicated that radiation can enhance the inter-diffusion between the SiC and carbon phases in SiC/SiC composite during the ions irradiation process at 300 °C [33]. However, these bright contrast small particles were also observed in the unirradiated area, which indicates that Si element were mixed in the PyC layer during the sample preparation process. Overall, it seemed that the ion irradiation has no significant influence on the PyC layer.

3.3. The behavior of the SiC matrix under irradiation

Fig. 8(a) shows that the SiC Coating layer has multiple layers, containing both nanocrystalline layers and columnar crystal layers. As shown in the high resolution image in Fig. 8(b), the microstructure of the nanocrystalline layer similar to that of the SiC fiber, consists of nano-grains with average size about 5 nm. The columnar crystal layer is mainly composed of 3C–SiC that grew along the [111] direction as the high resolution image in Fig. 8(c) shown. It contains many nanotwins and stacking faults. Such defects are corresponding to the elongation phenomenon of the diffraction spots in Fig. 8(d). (Elongation is normally from stacking faults that are planar defects. Twining gives mirrored diffractions). In fact, both the irradiated and unirradiated areas

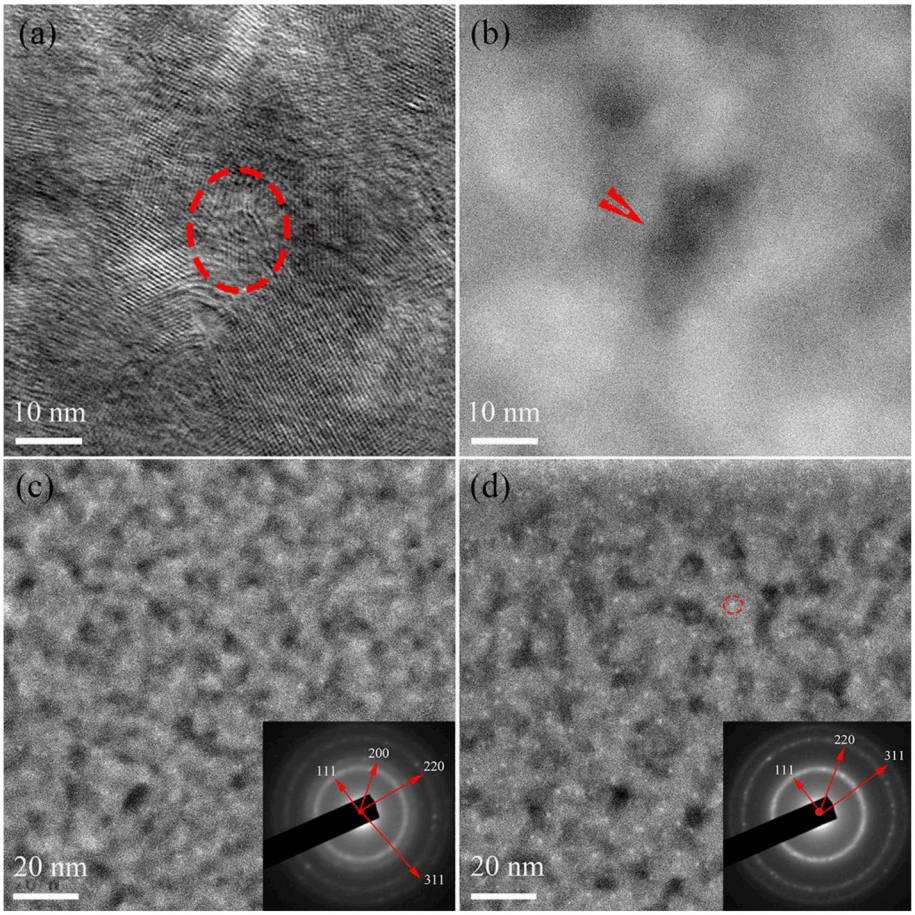

Fig. 5. STEM images of the SiC fiber (a) BF image; (b) HAADF image of the same area in (a); (c) HAADF image of the unirradiated fiber area, and the inserted image is the selected area electron diffraction pattern of the unirradiated region; (d) HAADF image of the irradiated fiber area, and the inserted image is the selected area electron diffraction pattern of the irradiated region.

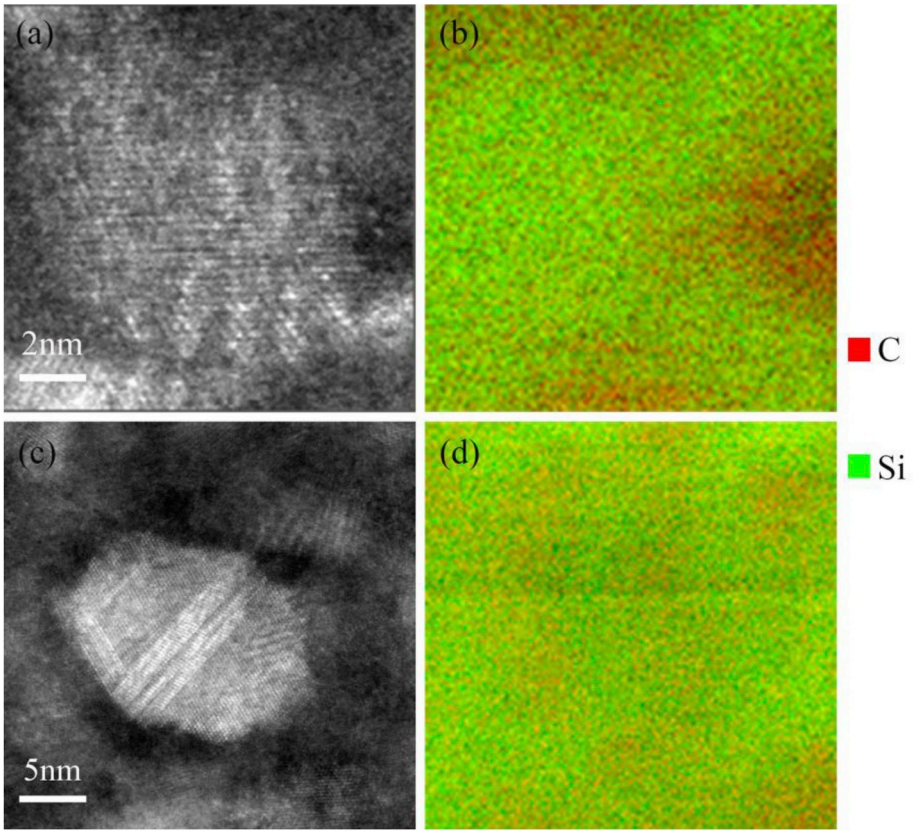

Fig. 6. Dark-field STEM images of the SiC fiber: (a) irradiated area; (b) is the EELS mapping results of (a); (c) unirradiated area; (d) is the EELS mapping results of (c).

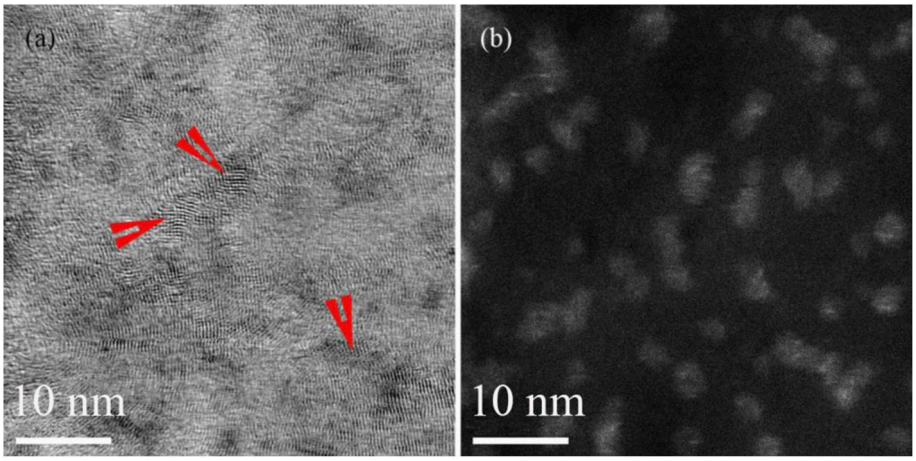

Fig. 7. STEM images of irradiated area in PyC interlayer (a) BF; (b) HAADF.

show similar diffraction features, and the high resolution images from these two areas both show that the original 3C–SiC columnar crystals also have a considerable amount of twins and stacking faults, which makes it difficult to explain whether the defects inside the columnar 3C–SiC grains were caused by irradiation.

As seen in Fig. 9(a), the SiC matrix is a complete polycrystalline crystal structure consisting of columnar crystal grains with the length ranging from 100 nm to 2000 nm and the height ranging from 20 nm to 200 nm. The defects inside the unirradiated grains are mainly the twins, just as Fig. 9(b) shows, and each layer of twins contains only about 3 atomic layers. The SiC fiber matrix still maintained a complete polycrystalline crystal structure and the grain size did not change significantly after irradiation for 90 dpa as the lattice structure is clearly visible. After ion irradiation, no significant microstructure changes were observed in low magnification images, such as dislocation loops [16] and voids [18]. However, from the high resolution image of Fig. 9(c), except twinning boundaries, only several dislocations can be observed, one of which is marked by red frame. Compared with the original unirradiated 3C–SiC matrix grains, the thickness of the twin layer increased after ion irradiation, which is marked by the double arrow red line in Fig. 9(c). The average number of atomic layers contained in each twin crystallization layer in the SiC grains in the irradiated and unirradiated areas were calculated to be 5 and 3, respectively. More than 50 grains were analyzed. In fact, the twins can grow

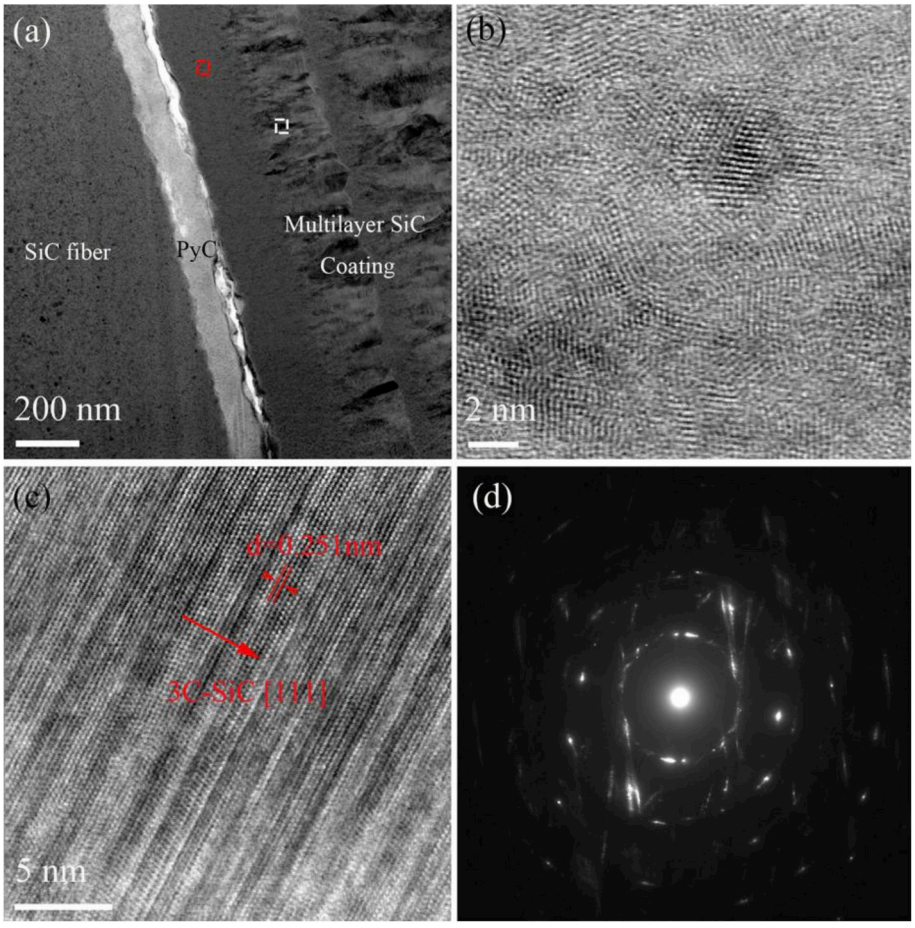

Fig. 8. STEM BF images of the irradiated area in multilayer SiC coating: (a) Overview image; (b) High resolution image from the red frame outlined area in (a); (b) High resolution image from the white frame outlined area in (a); (d) SAED pattern from the multilayer SiC Coating. (For interpretation of the references to colour in this figure legend, the reader is referred to the Web version of this article.)

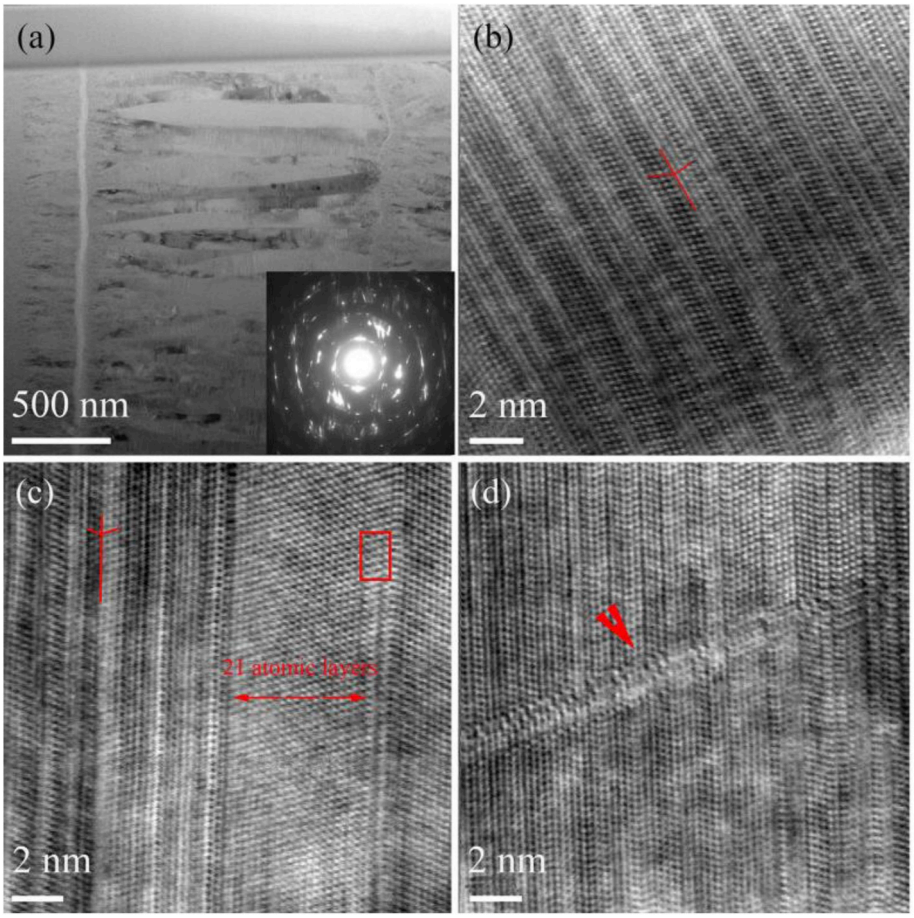

Fig. 9. STEM BF images of the SiC matrix: (a) Overview image; (b) High resolution image of one SiC grain in unirradiated area; (c) and (d) are high resolution images of two SiC grains in irradiated area, respectively.

up during the irradiation process due to the release of the energy of the twinning boundaries [34]. In addition, only one edge-on dislocation loop was found in this sample as shown in Fig. 9(d), which is located at the peak damage area in SiC matrix. As there are a large number of twinning boundaries inside the sample, which can absorb dislocations as traps to prevent the formation of large dislocation loops [35]. In addition, dislocation loops were only detected in the larger matrix grains by Weber et al. [16], which revealed a potential role of grain size on defect accumulation in SiC. So the small size of the matrix grains inside this new type SiC_f/SiC composite along the vertical direction of surface might also limit the growth and aggregation of defects. Overall, it is difficult to form dislocation loops in this new type SiC_f/SiC composite.

3.4. Nanohardness

The nanohardness of this SiC fiber-reinforced SiC matrix composites before and after Au ion irradiation was also measured with the results shown in Fig. 10. It can be seen from Fig. 10(a) that the depth of the hardness test is about 130 nm and the deepest part of the irradiation area is located at about 1300 nm (according to the SRIM simulation results), which can greatly avoid not only the influence of surface roughness, but also the impact of unirradiated area on the test results. Fig. 10(b) clearly shows the hardness changes of different parts in this SiC/SiC composite before and after irradiation. Before irradiation, the hardness of SiC matrix is significantly higher than SiC fiber. After irradiation, the hardness of the fiber has significantly increased while the hardness of the matrix has reduced slightly, which can be considered to remain unchanged due to the existence of measurement errors. In fact, hardness is a complex property which involves both elastic and plastic deformation, crack initiation and propagation, and the development of new surfaces. Generally, hardness is dependent on the fabrication process, composition, and the presence of impurities [36]. For unirradiated SiC_f/SiC composite, one of the reasons why the hardness of matrix is higher than the fiber can be expressed by the following formula [37]:

$$H = H_0 \exp(-CV_p) \quad (1)$$

where H is the hardness of SiC in GPa; H_0 is the hardness of a polycrystalline, high purity and very dense SiC material (assumed to be a pore-free SiC material); C is a constant, and V_p is the porosity of the material. As the fiber is a nano-polycrystalline structure while the matrix is a columnar crystal structure with larger average grain size, so the porosity of fiber is much higher than that of the matrix, which results in that the matrix has a higher hardness than the fiber. In addition, the excess carbon in the form of inter-granular packets was proved that it could reduce the hardness as impurities [1,16]. The significant hardness increase of SiC fiber after irradiation can be attributed to the pinning effect caused by irradiation-induced small point defects and small defect clusters [38]. One the other hand, the Au atoms dissolved in the SiC fiber might also have an effect on the hardness increase of the SiC fiber after irradiation. The hardness of the SiC matrix did not change significantly after irradiation, which is consistent with the STEM results that the atomic structure was almost stable after ion irradiation. The slight decrease in hardness of SiC matrix might be due to the decrease of twinning boundaries induced by irradiation, and the dislocation enhancement effect of irradiation is not sufficient to compensate for the contribution of the reduction in the number of twins to

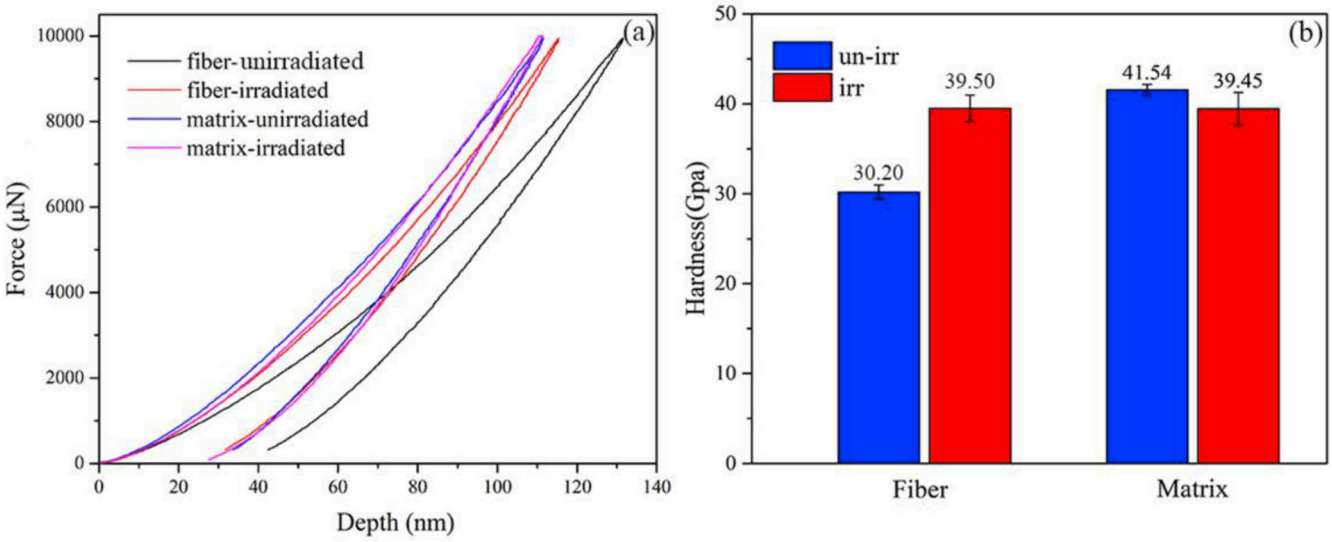

Fig. 10. The average hardness of fiber and matrix in SiC fiber-reinforced SiC matrix composites before and after ion irradiation.

hardness.

4. Conclusions

The microstructure and nanohardness of a SiC_f/SiC composite before and after ion irradiation were studied. It was revealed that irradiation had induced the enrichment of carbon at the grain boundaries in the fibers, which was due to reason that the C interstitials produced by irradiation migrated to the grain boundaries and combined with the original carbon packets. The disappearance of the {200} diffraction ring after irradiation indicates that a phase transition from 3C–SiC to Si has occurred due to the loss of C atoms in 3C–SiC. In addition, ion irradiation can lead to a significant radiation hardening effect in SiC fibers, which is due to the pinning effect caused by irradiation-induced small defect clusters. PyC interphase layer contains a large number of nanoparticles enriched in Si and irradiation had no significant effect on those particles. SiC matrix consists of columnar crystal grains with the length ranging from 100 nm to 2000 nm and the height ranging from 20 nm to 200 nm. Twins/stacking faculty are the main defects in matrix. Ion irradiation can lead to twin growth and thus a reduction in the number of twin boundaries. After ion irradiation up to 90 dpa, only a few dislocations and dislocation loops have been observed in the peak damage area in the SiC matrix. The hardness of SiC matrix did not change significantly after irradiation, which is consistent with the STEM results.

Acknowledgements

The support for this work was provided by CNPRI with the grant # 2015ZX06004001. Ion irradiation was conducted in the Michigan Ion Beam Laboratory (MIBL) located on the campus of the University of Michigan. Microstructure characterizations were conducted in the Michigan Center for Material Characterization (MC2) of the University of Michigan.

Appendix A. Supplementary data

Supplementary data to this article can be found online at https://doi.org/10.1016/j.ceramint.2019.12.044.

References

[1] Y. Zayachuk, P. Karamched, C. Deck, P. Hosemann, D.E.J. Armstrong, Linking microstructure and local mechanical properties in SiC-SiC fiber composite using micromechanical testing, Acta Mater. 168 (2019) 178–189.
[2] X. Jing, X.G. Yang, D.Q. Shi, H.W. Niu, Tensile creep behavior of three-dimensional four-step braided SiC/SiC composite at elevated temperature, Ceram. Int. 43 (9) (2017) 6721–6729.
[3] T. Koyanagia, T. Nozawab, Y. Katoha, L.L. Snead, Mechanical property degradation of high crystalline SiC fiber-reinforced SiC matrixcomposite neutron irradiated to ~100 displacements per atom, J. Eur. Ceram. Soc. 38 (2018) 1087–1094.
[4] M. Bosi, C. Ferrari, D. Nilsson, P.J. Ward, 3C-SiC carbonization optimization and void reduction on misoriented Si substrates: from a research reactor to a production scale reactor, CrystEngComm 39 (2016) 7478–7486.
[5] F. Linez, E. Gilabert, A. Debelle, P. Desgardin, M.-F. Barthe, Helium interaction with vacancy-type defects created in silicon carbide single crystal, J. Nucl. Mater. 436 (1–3) (2013) 150–157.
[6] S. YAJIMA, J. HAYASHI, M. OMORI, K. OKAMURA, Development of a silicon carbide fibre with high tensile strength, Nature 261 (1976) 683–685.
[7] J.L. Qi, Q. Eri, B. Kong, Y.F. Zhang, The normal spectral emittance of the real surface from worked aero-engine nozzle, Appl. Therm. Eng. 150 (2019) 641–650.
[8] W. Li, K. Shirvan, ABAQUS analysis of the SiC cladding fuel rod behavior under PWR normal operation conditions, J. Nucl. Mater. 515 (2019) 14–27.
[9] H. Mei, Z.Y. Kong, J.C. Xia, L.F. Cheng, S.S. Fan, Quantitative characterization of nanoindentation properties of CVI gradient SiC ceramic into CNT arrays, J. Alloy. Comp. 762 (2018) 196–202.
[10] J. Wang, X. Chen, K. Guan, L.F. Cheng, Y.S. Liu, Effects of channel modification on microstructure and mechanical properties of C/SiC composites prepared by LA-CVI process, Ceram. Int. 44 (14) (2018) 16414–16420.
[11] F.H. Gern, Liquid silicon infiltration: description of infiltration dynamics and silicon carbide formation, Composites Part A (28A) (1997) 355–364.
[12] R.M. Sullivan, E.H. Baker, C.E. Smith, G.N. Morscher, Modeling the effect of damage on electrical resistivity of melt-infiltrated SiC/SiC composites, J. Eur. Ceram. Soc. 38 (15) (2018) 4824–4832.
[13] M. Caccia, C.C. Xiang, J. Narciso, N. Gupta, Reactive melt infiltration as synthesis route for enhanced SiC/CoSi2 composite materials for advanced armor systems, Ceram. Int. 44 (11) (2018) 13182–13190.
[14] R.J. He, G.J. Ding, K.Q. Zhang, Y. Li, D.N. Fang, Fabrication of SiC ceramic architectures using stereolithography combined with precursor infiltration and pyrolysis, Ceram. Int. 45 (11) (2019) 14006–14014.
[15] U. Santoro, E. Novitskayaa, K. Karandikara, H.E. Khalifa, O.A. Graevea, Phase stability of SiC/SiC fiber reinforced composites: the effect of processing on the formation of α and β phases, Mater. Lett. 241 (15) (2019) 123–127.
[16] S. Agarwal, G. Duscher, Y. Zhao, M.L. Crespillo, Y. Katoh, W.J. Weber, Multiscale characterization of irradiation behaviour of ion-irradiated SiC/SiC composites, Acta Mater. 161 (2018) 207–220.
[17] S. Kondo, T. Hinoki, M. Nonaka, K. Ozawa, Irradiation-induced shrinkage of highly crystalline SiC fibers, Acta Mater. 83 (15) (2015) 1–9.
[18] M. Li, X. Zhou, H. Yang, S. Du, Q. Huang, The critical issues of SiC materials for future nuclear systems, Scr. Mater. 143 (15) (2018) 149–153.
[19] T. Koyanagia, T. Nozawab, Y. Katoha, L.L. Snead, Mechanical property degradation of high crystalline SiC fiber-reinforced SiC matrix composite neutron irradiated to ~100 displacements per atom, J. Eur. Ceram. Soc. 38 (2018) 1087–1094.
[20] L.W. Yang, H.T. Liu, H.F. Cheng, Processing-temperature dependent micro- and macro-mechanical properties of SiC fiber reinforced SiC matrix composites, Composites Part B 129 (2017) 152–161.
[21] Q. Huang, G.H. Lei, R.D. Liu, J.J. Li, L. Yan, C. Li, W.H. Liu, M.H. Wang, Microstructure, hardness and modulus of carbon-ion-irradiated new SiC fiber (601-4), J. Nucl. Mater. 503 (2018) 91–97.
[22] L.H. Karlsson, A. Hallén, J. Birch, L. Hultman, P.O.Å. Persson, Atomically resolved microscopy of ion implantation induced dislocation loops in 4H-SiC, Mater. Lett. 181 (2016) 325–327.

[23] W. Liu, L.F. Cheng, Y.G. Wang, H.J. Ma, Investigation of the residual stress in reaction-bonded SiC under irradiation, J. Eur. Ceram. Soc. 36 (16) (2016) 3901–3907.
[24] B. Michaut, T. Jourdan, J. Malaplate, A. Renault-Laborne, F. Sefta, B. Decamps, Cluster dynamics modeling and experimental investigation of the effect of injected interstitials, J. Nucl. Mater. 496 (2017) 166–176.
[25] V. Amandine, M. Cédric, M. Sergio, D. Patriciae, An ImageJ tool for simplified post-treatment of TEM phase contrast images (SPCI), Micron 121 (2019) 90–98.
[26] M. Song, C. Sun, Y.X. Chen, Z.X. Shang, X.H. Zhang, Grain refinement mechanisms and strength-hardness correlation of ultra-fine grained grade 91 steel processed by equal channel angular extrusion, Int. J. Press. Vessel. Pip. 172 (2019) 212–219.
[27] P.A. Midgley, M. Weyland, L. Laffont, J.M. Thomas, Z-contrast HAADF-STEM tomography, Microsc. Microanal. 9 (S02) (2003) 178–179.
[28] D. Frazer, M.D. Abad, D. Krumwiede, C.A. Back, H.E. Khalifa, C.P. Deck, P. Hosemann, Localized mechanical property assessment of SiC/SiC composite materials, Composites Part A 70 (2015) 93–101.
[29] M. Ayedh, R. Nipoti, A. Hallén, B.G. Svensson, Elimination of carbon vacancies in 4H-SiC employing thermodynamic equilibrium conditions at moderate temperatures, Appl. Phys. Lett. 107 (2015) 252102.
[30] M. Bockstedte, A. Mattausch, O. Pankratov, Ab initio study of the migration of intrinsic defects in 3C-SiC, Phys. Rev. B Condens. Matter 68 (20) (2003) 205201.
[31] A.G. Perez-Bergquist, T. Nozawa, C. Shih, K.J. Leonard, L.L. Snead, Y. Katoh, High dose neutron irradiation of Hi-Nicalon Type S silicon carbide composites, Part 1: microstructural evaluations, J. Nucl. Mater. 462 (2015) 443–449.
[32] N. Nakazato, H. Kishimoto, J. Park, Appropriate thickness of pyrolytic carbon coating on SiC fiber reinforcement to secure reasonable quasi-ductility on NITE SiC/SiC composites, Ceram. Int. 44 (16) (2018) 19307–19313.
[33] S. Kondo, T. Hinoki, M. Nonaka, K. Ozawa, Irradiation-induced shrinkage of highly crystalline SiC fibers, Acta Mater. 83 (2015) 1–9.
[34] J. Li, D.Y. Xie, S. Xue, C. Fan, Y. Chen, H. Wang, J. Wang, X. Zhang, Superior twin stability and radiation resistance of nanotwinned Ag solid solution alloy, Acta Mater. 151 (2018) 395–405.
[35] P. Chen, F.X. Wang, B. Li, Dislocation absorption and transmutation at {10-12} twin boundaries in deformation of magnesium, Acta Mater. 164 (2019) 440–453.
[36] L.L. Snead, T. Nozawa, Y. Katoh, T. Byun, S. Kondo, D.A. Petti, Handbook of SiC properties for fuel performance modeling, J. Nucl. Mater. 371 (2007) 329–377.
[37] E. Ryshkewitch, Compression strength of porous sintered alumina and zirconia: 9th communication to ceramography, J. Am. Ceram. Soc. 36 (1953) 65–68.
[38] J.J. Li, H.F. Huang, G.H. Lei, Q. Huang, R.D. Liu, D.H. Li, L. Yan, Evolution of amorphization and nanohardness in SiC under Xe ion irradiation, J. Nucl. Mater. 454 (2014) 173–177.